Strongly inhibited spontaneous emission of PbS quantum dots covalently bound to 3D silicon photonic band gap crystals

Andreas S. Schulz,[†,‡,¶] Marek Kozoň,[†,§] G. Julius Vancso,[¶,‖] Jurriaan Huskens,[‡] and Willem L. Vos[*,†]

†*Complex Photonic Systems (COPS), MESA+ Institute, University of Twente, P.O. Box 217, 7500 AE Enschede, The Netherlands*
‡*Molecular Nanofabrication (MNF), MESA+ Institute, University of Twente, P.O. Box 217, 7500 AE Enschede, The Netherlands*
¶*Materials Science and Technology of Polymers (MTP), MESA+ Institute, University of Twente, P.O. Box 217, 7500 AE Enschede, The Netherlands*
§*Mathematics of Computational Science (MACS), MESA+ Institute, University of Twente, P.O. Box 217, 7500 AE Enschede, The Netherlands*
‖*Sustainable Polymer Chemistry (SPC), MESA+ Institute, University of Twente, P.O. Box 217, 7500 AE Enschede, The Netherlands*

E-mail: w.l.vos@utwente.nl

Abstract

We present an optical study of the spontaneous emission of lead sulfide (PbS) nanocrystal quantum dots in three-dimensional (3D) photonic band gap crystals made from silicon. The nanocrystals emit in the near infrared (NIR) range to be compatible with the 3D silicon nanophotonics. The nanocrystals are covalently bonded to polymer brush layers that are grafted from the Si-air interfaces inside the nanostructure using surface-initiated atom transfer radical polymerization (SI-ATRP), and their presence and position of the quantum dots was previously characterized by synchrotron X-ray fluorescence tomography. We report both continuous wave emission spectra and time-resolved time-correlated single photon counting. In time-resolved measurements, we observe that the total emission rate greatly increases when the quantum dots are transferred from suspension to the silicon nanostructures, likely due to quenching (or increased non-radiative decay) that is tentatively attributed to the presence of Cu-catalyst during the synthesis. In this regime, continuous wave (cw) emission spectra are known to be proportional to the radiative rate and thus to the local density of states. In spectra normalized to those taken on flat silicon outside the crystals, we observe a broad and deep stop band that we attribute to a 3D photonic band gap with a relative bandwidth up to 26%. The shapes of the relative emission spectra match well with the theoretical density of states spectra calculated with the plane wave expansion. The observed inhibition is 5 to 30 times, similar to previously reported record inhibitions, yet for completely coincidental reasons. Our results are relevant to applications in photochemistry, sensing, photovoltaics, and to efficient miniature light sources.

Introduction

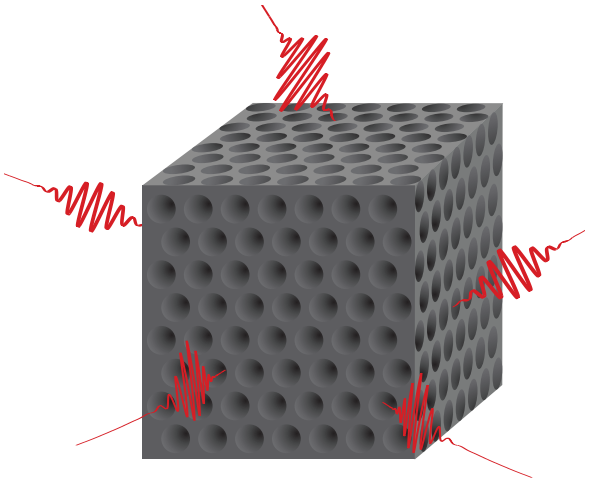

Figure 1: Cartoon of a finite three-dimensional (3D) photonic crystal in free space. Since the crystal has a complete 3D photonic band gap, ubiquitous vacuum fluctuations incident on the crystal's surface (shown as red wavelets) are forbidden from entering and reflect from the crystal's surfaces. Hence, an excited two-level quantum system (atom, ion, molecule, or quantum dot) embedded inside the crystal is shielded from the fluctuations and cannot decay by spontaneously emitting a photon. Thus, the excited state becomes more stable.

The intriguing opportunity to control the properties of matter via the properties of light lies at the heart of quantum optics and cavity quantum electrodynamics (cQED). A famous example is the control of the radiative rate of an elementary quantum emitter such as an excited atom, ion, molecule, 2D material, or quantum dot.[1] Such control is essential for applications ranging from miniature lasers and light-emitting diodes,[2,3] to single-photon sources for quantum information,[4–6] solar energy harvesting,[7,8] to photocatalysis and photochemistry,[9–11] and sensing.[12,13]

When the emitter's properties are in the quantum regime, as is the case with nanoemitters in the optical range, a major role is played by the fluctuations of the quantized electromagnetic field called vacuum fluctuations.[14,15] Figure 1 shows a schematic illustration of such fluctuations that even exist when there are no photons. By surrounding an emitter by a suitably tailored dielectric environment, the vacuum fluctuations are controlled; a most radical control is a photonic band gap as discussed in this paper, where all light and thus also all vacuum fluctuations are forbidden by interference, as illustrated in Figure 1.

Long after the pioneering realization by Purcell that an emitter's environment such as a cavity controls the emission rate,[16] emission control has become one of the main drivers of the field of nanophotonics.[17–21] Following seminal work by Bykov and by Yablonovitch,[1,2] emission control was first studied on periodic photonic crystals,[22–32] and recently even extended to 3D circuits[33] and chiral emission.[34] Emission control has also successfully been pursued with many different nanophotonic systems and many different quantum emitters, for instance, atoms and dye molecules in Fabry–Pérot microcavities,[35,36] quantum dots in pillar microcavities[5,37] and in disordered photonic materials,[38] ions in whispering gallery-mode microspheres,[39–41] dye molecules in plasmonic nanocavities and on nanoantennae,[42–46] dye molecules in metamaterials,[47,48] diamond and perovskite nanocrystals in photonic crystals.[49,50]

In the weak-coupling approximation in cQED, also known as the Wigner-Weisskopf approximation,[51] spontaneous emission of an excited quantum emitter is precisely described by Fermi's golden rule;[52] in a modern reformulation the radiative decay rate is linearly proportional to the local density of optical states (LDOS). The LDOS is a classical property that represents the density of vacuum fluctuations, and thus the amount of vacuum noise experienced by a qubit.[53] In a quantum electrodynamic view, vacuum fluctuations stimulate an excited quantum system to decay from its excited state, thereby impeding the quantum functionality that is often available with excited states.[1] The LDOS not

[1] It is well-known that vacuum fluctuations contribute only one half of the emission rate, the other

only controls spontaneous emission and blackbody radiation, but also plays a role in Van der Waals and Casimir dispersion forces between nanoparticles and in Förster resonant energy transfer (FRET) between different emitters.[54]

Expressed in words, the LDOS counts the number of electromagnetic field states available for emission, where each state is weighted by its strength at the emitter's position $\mathbf{r}_0$ and the field is projected along the emitter's dipole axis.[21,55,56] Figure 2(a) shows the frequency dependence of the DOS (the position and orientation-averaged LDOS) for a 3D photonic band gap crystal as studied here. *Grosso modo*, the DOS increases quadratically with frequency. In the reduced frequency range $\tilde{\omega} \equiv a/\lambda = 0.54$ to 0.68 (with a the lattice parameter and λ the wavelength) the DOS is completely inhibited,[56–63] which defines the complete 3D photonic band gap [2]. In the photonic band gap, the vacuum fluctuation wavelets in Figure 1 are portrayed to bounce off the crystal external surface. Outside the gap, the DOS is enhanced in a number of peaks since the total number of states is conserved. For comparison, the DOS of a homogenized medium with the same effective refractive index as the crystal matches in the low-frequency range to about $\tilde{\omega} = 0.25$ before further increasing quadratically. The DOS of free space is also quadratic like the effective medium, albeit overall much lower since the DOS is proportional to the (effective) refractive index cubed.[21]

Figure 2(b) shows the photonic crystal's relative DOS that is normalized to the DOS of the effective homogeneous medium for two reasons: Firstly, it is insightful to remove the parabolic dependence, hence an unmodified DOS corresponds to a relative DOS equal to one, enhancements correspond to a relative

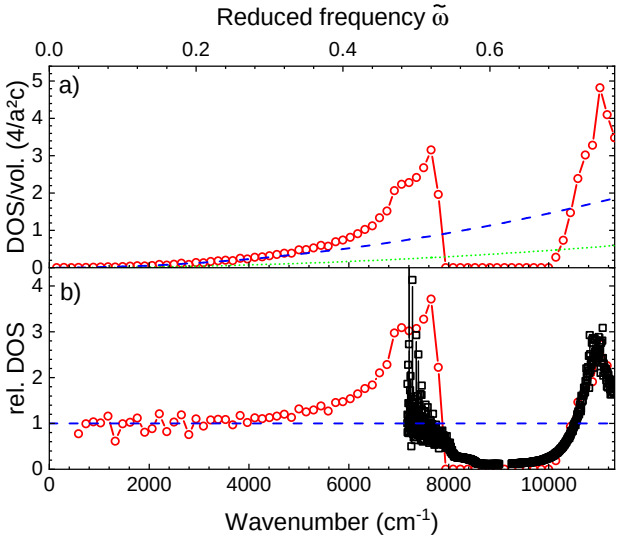

Figure 2: Density of photonic states. a) Density of states (DOS) reduced by the lattice parameter a and the speed of light c for an inverse woodpile photonic band gap crystal made from silicon ($\epsilon = 11.7$) calculated (red circles) for pores with reduced radii $R/a = 0.252$. The top abscissa indicates the reduced frequency proportional to the lattice parameter over the wavelength a/λ. The blue dashed line is the DOS of a homogeneous medium with the same effective refractive index as the crystal, and the green dotted curve the DOS of free space. (b) Relative DOS equal to the DOS of the crystal over the DOS of the effective medium (red circles.) Black squares show our main result, namely the measured intensity of quantum dots inside a 3D silicon photonic crystal normalized to the intensity of similar quantum dots on a silicon surface, and reveal a broad band gap with strong inhibition. The red circles are the DOS (shown in (a)) normalized to a homogeneous medium with the same low-frequency behavior (see (a)) with the horizontal dashed blue line representing relative DOS = 1, that is, the unmodified DOS.

half being induced by electrodynamical back action, see.[15,21]

[2]We express frequency as a reduced frequency $\tilde{\omega} = \omega a/(2\pi c))$, with ω the frequency, a the lattice parameter, and c the speed of light (not to be confused with the lattice parameter in the Y direction). The reduced frequency $\tilde{\omega}$ also equals (a/λ) which is convenient in the interpretation of experiments.

DOS > 1 and inhibitions to a relative DOS < 1. Secondly, the ratio is a model of experiments as in this paper, where we normalize the intensity collected from quantum emitters (such as quantum dots) inside a photonic crystal to the intensity of similar emitters in a reference situation without band gap. By such a procedure, we normalize out the spectrum specific of the emitters in order to focus on the crystal properties. Similar procedures were used in previous work, where the effect of band gap crystals was studied on laser dye molecules and quantum wells.[25,26] The black squares show the main result of the present paper, namely the measurements of one of our 3D silicon photonic band gap crystals with quantum dots as internal quantum emitters. We find a broad range of strongly inhibited emission between about 8000 to 10400 cm^{-1}, characteristic of a 3D photonic band gap with a relative bandwidth (width over center frequency) of about 26%, which matches well with the theoretical relative DOS.

Therefore, in this paper we present a detailed optical study of quantum dots that are located on polymer brush layers that are grafted to the Si-air interfaces inside the 3D nanostructure using surface-initiated atom transfer radical polymerization (SI-ATRP).[64,65] We compare both the spectra and excited-state lifetimes in our crystals that were previously characterized by non-destructive X-ray fluorescence tomography.[66]

Experimental section

3D silicon photonic crystals

We study 3D photonic band gap crystals made from silicon with the diamond-like inverse woodpile structure that consists of two perpendicular arrays of interpenetrating pores. Figure 3 shows a SEM image of a successfully etched photonic band gap crystal. The pores that enter into the XY surface (top) and into the XZ surface (bottom) mutually cross inside the Si beam and thereby form the 3D tetragonal inverse woodpile structure with a width of about 10 micron that has a broad 3D photonic band gap.[67–69]

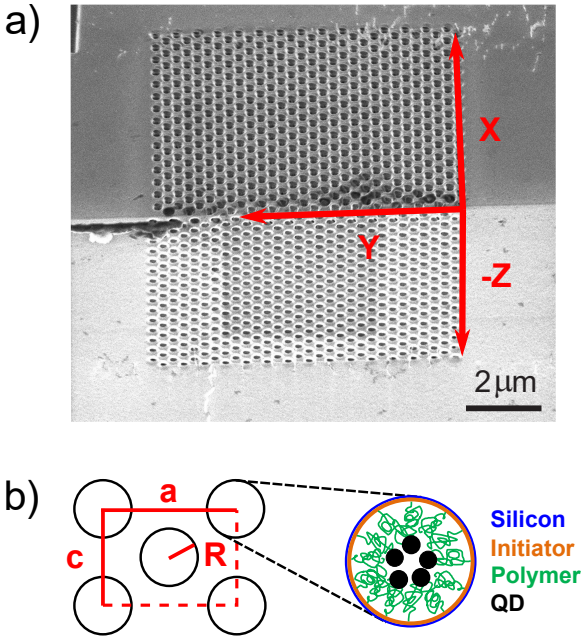

Figure 3: (a) Scanning electron micrograph (SEM) of a 3D photonic band gap crystal viewed from 45° on the edge of the silicon beam showing the XY (top) and the XZ surfaces (bottom); the scale bar indicates 2 μm. (b) View along the pores showing the lattice parameters a, c (with $a = \sqrt{2}c$), and pore radius R. Zoomed-in cross-section of one pore with targeted polymer surface-chemistry: ATRP initiator layer (orange), polymer chains forming brushes (green), and covalently attached PbS quantum dots (black) on top of silicon (blue).

The crystals are designed to have a lattice parameter $a = 680$ nm and pore diameters of $d = 260$ or 320 nm. The pore diameters correspond to reduced radii of $R/a = 0.191$ and 0.235. From Figure 2 it is apparent that in this range of pore radii the 3D photonic band gap occurs between 8000 and 10000 cm^{-1} in the near infrared spectral range (see also[69]).

Quantum dots positioned by surface chemistry

As internal emitters, we choose near-infrared emitting lead sulfide quantum dots whose

emission band includes telecom bands and is compatible with the transparency range of silicon below the electronic band gap at 1.1 eV corresponding to wavelengths shorter than 1100 nm (see, *e.g.*, Ref.[8]). In addition, quantum dots were chosen to have their emission spectrum overlap with the 3D photonic band gap, shown in Figure 2.

To position the quantum dots inside the crystals, a thin polymer brush layer was grafted inside the pores of the 3D silicon photonic band gap crystals to attach lead sulfide quantum dots. The inorganic lead sulfide core of the quantum dots is covered by a poly(ethylene glycol)-amine (PEG-NH_2) ligand that is used to couple to the polymer layer on the silicon photonic crystal.[66]

Optical setup

The optical microscope setup to collect both spectrally-resolved and time-resolved spontaneous emission from the near IR quantum dots inside the 3D photonic band gap is described in detail in the Supporting Information. In many collected spectra, a narrow range around 9100 cm^{-1} is absent since the involved diode array detector has a number of so-called "dead" pixels.

Results and discussion

Emission spectra

Figure 4 shows emission spectra of the quantum dots in suspension and of quantum dots attached with polymer brushes to the flat silicon substrate adjacent to the photonic crystals. In suspension, the quantum dot emission maximum is observed at 9610 cm^{-1}, which corresponds to a lead sulfide quantum dot diameter of about $d = 3.46$ nm.[70] The width is about 1315 cm^{-1} full width at half maximum (FWHM), mostly due to size polydispersity,[71] and the maximum intensity is nearly 100 counts/s. The spectra of the quantum dots attached to the silicon surface have a maximum near 8900 cm^{-1}, which is red shifted by about 710 cm^{-1} compared to the dots in suspension. The FWHM of the emission spectra on the surface is about 1070 cm^{-1}, somewhat narrower than in suspension.

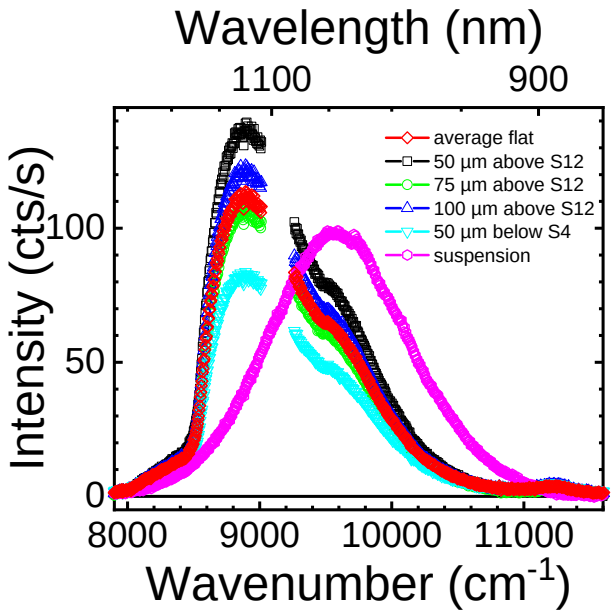

Figure 4: The emission spectrum of the PbS quantum dots in suspension is shown as magenta hexagons. The emission spectra of the quantum dots at four locations on the flat silicon surface on bar 3DPC1 are shown as black, blue, green and teal symbols, with the average spectrum shown as red diamonds.

We attribute the apparent shift and narrowing to two main features: firstly, the quantum dots experience different dielectric environments, where the dots in suspension are in water with an optical dielectric function of about $\epsilon_{sus} = 1.69$.[72] On the silicon-air surface the dots experience a dielectric function $\epsilon_{Si} = 12$ on the Si side and $\epsilon_{air} = 1$ on the air side, which we interpret as an effective medium with $\epsilon_{med} = \frac{\epsilon_{Si}+\epsilon_{air}}{2} = 6.5$, which is substantially greater than in suspension. In a high-epsilon environment two-level emitters generally emit at a lower emission frequency due to the increased polarization of the environment by the emitting dipole,[73,74] which qualitatively agrees with our observations in Figure 4. Secondly, in suspension the quantum dots are well separated whereas on the flat silicon surface they are in close vicinity

due to the densification from a 3D chemical reaction environment to a 2D surface. Consequently, we surmise that the dots on the surface experience energy transfer, including Förster Resonant Energy Transfer (FRET),[73,75] whereas the dots in suspension do not. In case of energy transfer, high-frequency "blue-emitting" quantum dots effectively transfer their excitation to more red-emitting dots, hence the apparent enhancement of the low-frequency part of an emission spectrum at the expense of the high-frequency side. Such an enhancement of the red side and simultaneous decrease of the blue side of the spectrum agrees qualitatively with the observations in Figure 4.

Insights into effects of the employed brush surface chemistry are obtained by comparing the emitted intensity collected from different areas on the flat silicon surface, by scanning the excitation laser spot across sample 3DPC1, where the length scale of the probe is given by the focal diameter of the excitation laser (about 1 μm). The intensity maxima range from 83 to 139 cts/s, corresponding to less than $\pm$25% relative change from the average, which is a fairly small variation of absolute intensities, which indicates that the coverage with quantum dots is fairly homogeneous across the silicon surface. This micron-scale homogeneity is attributed to the covalent attachment of the QDs to the polymer brushes that generally leads to a homogeneous and well-controlled coverage. For comparison, in sample 3DPC2 the quantum dots were not covalently attached to the polymer layer, but physisorbed. Here, the intensities fluctuate much more while scanning the excitation laser across the sample, namely between 390 and 12600 counts/s (more than 30 times), thus much more than above. We attribute the larger variations to aggregation of quantum dots in patches with few or even many dots clumped together.

Previously, we have probed the location of the quantum dots inside the photonic crystals with high spatial resolution (few tens of nanometers) by synchrotron X-ray fluorescence tomography,[66] on the same samples as studied here, especially 3DPC1. In the tomography study, we found that the detailed distribution of individual quantum dots shows some inhomogeneity along the length of each pore. However, averaged over the length of pores (several microns) the distribution of quantum dots is highly reproducible and homogeneous, which agrees with the optical probing above. From these observations combined we conclude that the coupling strategy using the brush surface chemistry developed here is a successful one for silicon-based functional samples since the infiltration of the quantum dots into the photonic crystal nanostructures is homogeneous on optically relevant length scales.

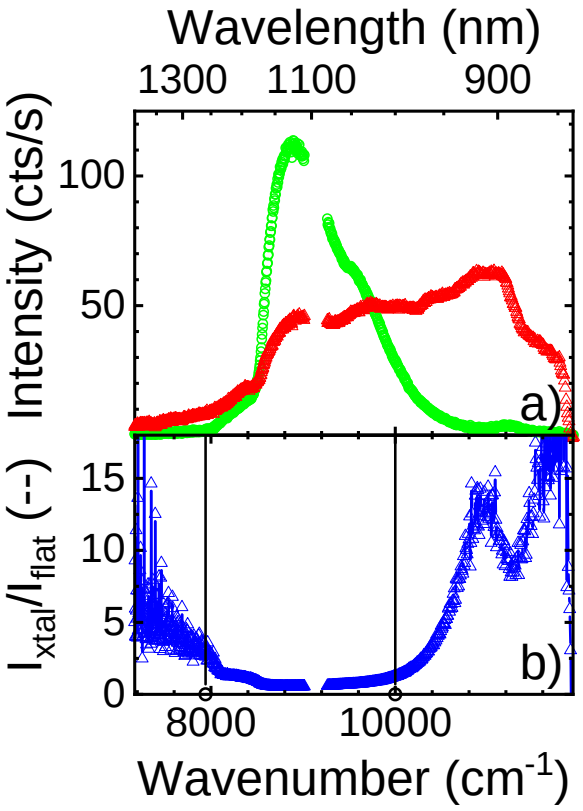

Figure 5: (a) Emitted intensity in counts/s versus photon energy (in wavenumbers, bottom abscissa) and wavelength (top abscissa) of quantum dots in crystal S12 on silicon bar 3DPC1 (red triangles). The green circles indicate the average spectrum of quantum dots on a flat silicon surface. (b) Ratio of the crystal to reference spectrum on a flat surface (blue triangles). The estimated band gap edges are shown as vertical black lines.

Figure 5(a) shows the emission spectrum of the quantum dots infiltrated in a 3D photonic band gap crystal and for comparison the spectrum taken on a flat substrate, where the dots were in both cases attached by the same chemical procedure. The spectrum on the flat silicon surface has an emission maximum at 8900 cm^{-1} and a shoulder at 9600 cm^{-1}, as in Figure 4. The spectrum of the quantum dots inside the photonic crystal is dramatically modified with respect to the spectrum on the silicon surface (and also compared to the suspension): the emission maximum has shifted to around 11000 cm^{-1}; in the frequency range around 9000 to 10000 cm^{-1} where quantum dots on Si (and in suspension) show emission maxima, the emission from inside the crystal is strongly inhibited. In addition to different spectral shapes, there are also other remarkable differences in emitted signal: in the frequency window between 8500 and 9750 cm^{-1} the quantum dots in the crystal have a considerably lower count rate; in the low frequency range below 8500 cm^{-1} the quantum dots in the crystal have a similar count rate as on the substrate, and above 9750 cm^{-1} the count rate is greater.

To discern the effect of the crystal on the emission spectrum, we show in Figure 5(b) the ratio of the silicon photonic crystal spectrum and the reference spectrum taken on the flat silicon substrate. This relative intensity spectrum shows a broad inhibition range between about 8000 and 10000 cm^{-1} that agrees with the photonic band gap expected from the DOS calculations. At low photon energies, the relative intensity decreases with wave number increasing to the gap, and above the gap, the relative intensity increases, while showing a marked peak at 10800 cm^{-1} that matches the peak in the DOS spectrum in Figure 2(a), and a further increase to 12600 cm^{-1}. The relative intensity in Figure 5(b) varies up to 15 in the peak at 10800 cm^{-1}, which differs from the relative intensity in the calculated relative DOS in Figure 2(b) that equals about 2.5 at the same peak. Several reasonable yet competing explanations for the overall difference in scale factor include: (i) a possible difference in areal density between quantum dots on the flat substrate versus those inside the curved pores, (ii) a possible difference in total number of quantum dots on the flat substrate versus inside the pores (due to different layer thickness), (iii) a possible difference in optical collection efficiency between the flat substrate (well defined focus) versus the photonic crystal where above-gap excitation light will be strongly scattered.[76] Since it is at this time not possible to conclusively quantify these explanations, we scale each measured relative intensity spectra by a single scale factor such that the peak at 10800 cm^{-1} matches the calculated one, where the resulting factors are listed in Table S5 of the Supporting Information.

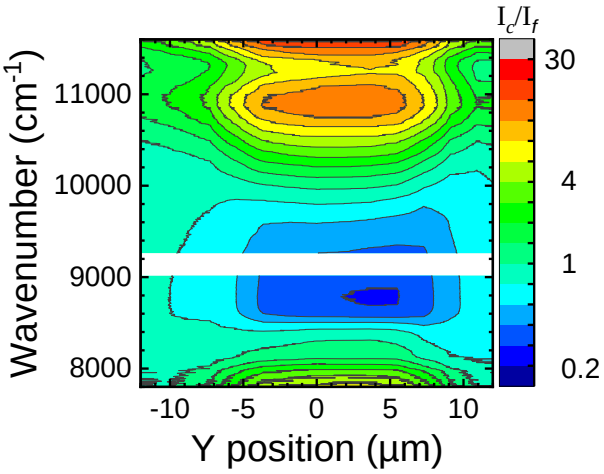

Figure 6: Spectral and Y position map of the emission inhibition for quantum dots in crystal S12 on silicon bar 3DPC1, obtained from spectra taken at 23 positions. The color map shows the inhibition defined as the ratio of a Y-dependent spectrum taken on the crystal and the flat Si surface reference spectrum (I_c/I_f). Green color ($I_c/I_f \simeq 1$) indicates no inhibition, blue ($I_c/I_f < 1$) is inhibited, and green, orange, red ($I_c/I_f > 1$) are enhanced.

For the same photonic crystal S12 as probed in Figure 5, we performed a position-dependent scan (in the Y direction parallel to the crystal-air interface) to verify that the inhibited emission indeed correlates with the presence of the photonic band gap crystal. The ratio of the intensity of the quantum dots

in and near the photonic band gap crystal to the intensity on the substrate far away from the crystal (I_c/I_f) is plotted in Figure 6 as a map versus frequency and Y position. Far away from the crystal this ratio closely equals 1 at all frequencies. The emission is observed to be most strongly inhibited at the center of the crystal at $Y = 4$ μm, in agreement with recent theoretical position-dependent calculations of the local density of states.[77] The inhibition extends over 10 μm which is in agreement with the crystal extent shown in Figure 3(b).

The inhibition smoothly decreases towards the edges of the photonic crystal, due to the finite size of the illuminating pulsed diode laser. In the same Y range where the crystal reveals inhibited emission, there is also a substantial enhanced emission near 11000 cm^{-1}, that matches with the theoretically predicted DOS peak at reduced frequency $\tilde{\omega} \equiv a/\lambda = 0.76$ in Figure 2(a). At both higher wave numbers near 12000 cm^{-1} and lower wave numbers near 7500 cm^{-1} there is additional enhanced emission, but due to the limited emission range of the quantum dots no clear features can be identified that can be compared to the theoretical DOS.

From the major differences between the spectra collected from the crystal versus the one on silicon, it is clear that the 3D photonic band gap crystal has a dramatic influence on the emission of the quantum dots. We discuss several possible hypotheses why the quantum dots reveal a major inhibition in their emission spectra when they are placed inside a 3D photonic band gap crystal, namely (1) a Franz-Keldish effect, (2) Förster Resonant Energy Transfer (FRET) from quantum dots to the silicon, (3) FRET between the quantum dots, (4) hot-electron transfer from the quantum dots to the silicon backbone, (5) a preferential infiltration of small quantum dots into the crystal pores, and (6) the presence of a 3D photonic gap.

The first hypothesis proposes that the emitted intensity is reduced due to an increased optical absorption, due to a Franz-Keldysh effect whereby the quantum dot's electron and hole wavefunctions increasingly "leak" into their electronic band gap.[74,78,79] Firstly, a strong electric field is necessary, which is absent in our experiments; secondly, the increased absorption reported in literature[74] is relatively weak and insufficient to explain a 5 to 30-times inhibition as described below; thirdly, the increased absorption occurs in the intrinsic absorption range of the quantum dots, which occurs at much higher photon energy than the photonic gap. Therefore, this hypothesis is so unlikely that we reject it.

The second hypothesis proposes that the quantum dots reveal FRET to the silicon backbone, as recently reported by Tabernig *et al.*[80] Firstly, the quantum dots are spaced from the silicon backbone by the polymer brush layer that has a thickness of 30 to 35 nm. While a quantum dot could possibly penetrate into the polymer brush layer, since we aimed for a high density polymer layer, it is unlikely that a quantum dot comes sufficiently close (1 to 10 nm) to the silicon surface to experience FRET. Moreover, the PbS quantum dots have a PEG-shell that further shields FRET. Secondly, FRET is usually associated with a red shifting of emission spectra,[73] which is not apparent at all in Figure 5(a), on the contrary, the spectra rather appear to show a blue shift for the crystal. Therefore, we find this hypothesis so unlikely that we reject it.

The third hypothesis proposes that the inhibition is caused by FRET between the quantum dots. FRET generally results in a red shift of the emission spectrum. Firstly, if there would be more FRET in the crystal, the relative spectrum would reveal a monotonous negative trend, and if there would be less FRET in the crystal, the relative spectrum would reveal a monotonous positive trend, Secondly, the quantum dots have a same chemical environment in the crystals as on the flat reference substrate, hence electron transfer seems equally likely on the reference samples, which corresponds to zero change in the relative intensity spectrum, in contrast to our observations. All three hypothesized spectral features do not match the observed inhibition, therefore we reject this FRET hypothesis.

The fourth hypothesis proposes that highly excited "hot" electrons inside the quantum dots may be transferred to a semiconductor backbone, see, *e.g.*, Tisdale *et al.*[81] Since the quantum dots have a similar chemical environment in the crystals as on the substrate, electron transfer seems equally likely on both samples, which corresponds to zero change in the relative intensity spectrum, in contrast to the observed inhibition. Therefore, we reject this hypothesis.

The fifth hypothesis proposes that the smaller quantum dots among the whole size population are preferentially infiltrated into the photonic crystal pores. Firstly, since the crystal pores have a diameter greater than 260 nm, whereas the quantum dots have much smaller diameters of about 3 to 6 nm, it is unlikely that steric effects affect infiltration. Secondly, a preferential infiltration of smaller dots would lead to an effective blueshift of the crystal spectrum compared to the reference, and thus to a relative spectrum with a monotonous positive trend, which does not match the observed inhibition, therefore we reject this hypothesis.

Finally the sixth hypothesis proposes that the strong spectral inhibition is caused by a 3D photonic band gap in the crystal. Indeed a gap is designed to be present in such crystals, see *e.g.* Ref.,[69,82] and below we report further support for this hypothesis, namely that the gap systematically shifts when crystal properties (here, the pore radii) are varied. Therefore, we sustain this hypothesis.

Comparison to photonic DOS

While the observation of a broad and strong inhibition that corresponds to the expected complete 3D photonic band gap in the photonic density of states is at this point remarkable and exciting, it is also surprising in view of our initial expectation that the quantum dots bound to the polymer brushes would have an elevated quantum efficiency.

From previous work[21,83,84] it is known that an important aspect in spontaneous emission control is the extent of the non-radiative decay (with rate Γ_{nonrad}) of the quantum emitter in comparison to the desired radiative decay (with rate Γ_{rad}). This extent is expressed by the quantum efficiency η that is equal to $\eta \equiv \Gamma_{\mathrm{rad}}/\Gamma_{\mathrm{tot}}$, where Γ_{tot} is the total emission rate equal to the sum of the radiative and the non-radiative rates $\Gamma_{\mathrm{tot}} = \Gamma_{\mathrm{rad}} + \Gamma_{\mathrm{nonrad}}$. It turns out that these properties decide whether the LDOS is apparent in either cw intensity spectra or in time-resolved observations. From the rate equation, the cw emitted intensity $I(\omega)$ (with spectra as in Figure 5 above) is derived to be:[83]

$$I(\omega) = P\frac{\Gamma_{\mathrm{rad}}(\omega)}{\Gamma_{\mathrm{rad}}(\omega) + \Gamma_{\mathrm{nonrad}}(\omega)}, \qquad (1)$$

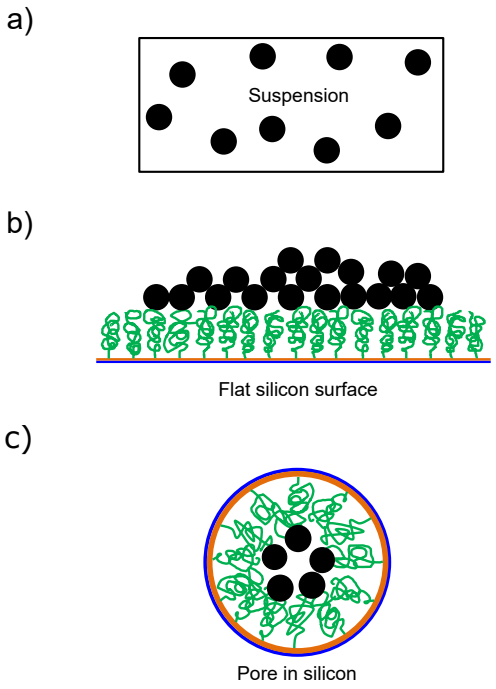

Figure 7: Schematic of how quantum dots are likely located in the three different sample studied here. (a) In suspension, the dots have a low density and are well-separated. (b) On a flat Si substrate, the QDs have a high areal density and are likely clustered or aggregated. (c) In a cross-section of a crystal pore the QDs have a medium high areal density and are separated thanks to the targeted brush polymer surface chemistry.

where P is the pump rate or excitation rate [3]. If emitters have a high quantum efficiency near unity ($\eta \simeq 1$) and hence $\Gamma_{rad} >> \Gamma_{nonrad}$, it follows from Eq. 1 that every incident pump photon is converted into an emitted photon ($I \simeq P$), hence the emitted intensity is independent of the LDOS. Conversely, if the emitters have a low quantum efficiency ($\eta << 1$, hence $\Gamma_{rad} << \Gamma_{nonrad}$), it follows from Eq. 1 that the intensity $I(\omega)$ is equal to

$$I(\omega) \simeq P \frac{\Gamma_{rad}(\omega)}{\Gamma_{nonrad}(\omega)}, \qquad (2)$$

which is proportional to the radiative rate, and thus to the LDOS.

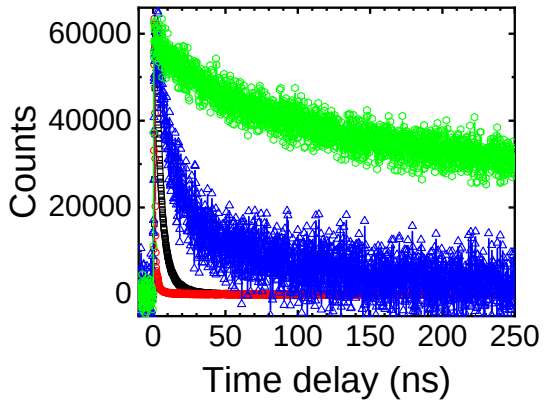

Figure 8: Time-correlated single photon counting of PbS quantum dots on sample 3DPC1 on a flat substrate (black squares), in crystal S4 (blue triangles), in crystal S12 (red circles), and in suspension (green hexagons, at 1090 nm^{-1}). The counts is plotted against the photon arrival time in ns.

To assess whether the quantum dots in our experiment are in the high or low efficiency limits, let us consider their microscopic placement in the various samples, illustrated in Figure 7, and time-resolved emission shown in Figure 8. In the suspension, the quantum dots have a low density (see Figure 7(a)), and are manufactured to have an as high as possible quantum efficiency. In time-resolved emission (Figure 8) the quantum dots show a decay with an emission rate of $\Gamma_{tot} = 0.223 \pm 0.004\ \mu s^{-1}$ in suspension, which matches with results in literature on good quality PbS quantum dots.[70,85,86] When the quantum dots are bound to the silicon substrate or inside the photonic crystal (see Figure 7(b, c)), it is reasonable that their local number density is much greater since during preparation the quantum dots are concentrated from volume to surfaces. Therefore, we expect the quantum dot-quantum dot quenching to be greater, hence a greater non-radiative rate. In addition, during the preparation the quantum dots are exposed to Cu catalyst that also increases the non-radiative rate.[87,88] In time-resolved emission (Figure 8), we observe that the quantum dots inside the 3D photonic crystals show much faster decay than in suspension. On the Si substrate, we find decay rates between $\Gamma_{tot} = 190.3 \pm 0.6$ and $\Gamma_{tot} = 267 \pm 0.6\ \mu s^{-1}$, and in the photonic crystal, we find $\Gamma_{tot} = 153.0 \pm 1.3\ \mu s^{-1}$ (see all data compiled in Table S4 of the Supporting Information. In other words, the decays in and on silicon are about 850 to 1200-fold greater than in suspension.

While one might optimistically surmise that a much faster decay is caused by an increased DOS or LDOS, we reject this hypothesis since the fast decay occurs both in the photonic crystal (major DOS modifications, see Figure 9) as well as on the Si substrate where DOS modifications are minor. Therefore, we conclude from the time-resolved decay and the physico-chemical considerations that the decay of the quantum dots on Si and in the photonic crystals is dominated by non-radiative decay. Therefore, we conclude that the emission spectra (see Figure 5) are in the low quantum efficiency limits, and hence the observed cw intensity spectra are proportional to the LDOS.

Emission spectra in photonic band gap crystals

Figure 9 shows the relative emission spectra of the PbS quantum dots infiltrated in the 3D silicon photonic band gap crystals with two

[3] Since the excitation occurs at a different (much higher) frequency, it is independent of the emission frequency ω.

different sets of pore radii, namely in panel (a) crystals with radii $R = 129$ nm (reduced radii $R/a = 0.19$) and in panel (b) with radii $R = 156$ nm (reduced radii $R/a = 0.23$). The emission spectra are referenced to those collected on flat Si substrates, to normalize out the specific spectrum of the quantum dots and thus concentrate on the local density of states of the crystals. Since the number of quantum dots and the collection efficiencies differ between the photonic crystals and the flat substrates, the count rates between these measurements may differ substantially, as discussed above (Figure 5). To allow for a comparison to theoretical results, we normalize the relative emission spectra such that the broad peak at 11000 cm^{-1} overlaps with the corresponding peak in the theoretical relative DOS spectra, with normalization constants provided in the Appendix. The reason for this procedure is that ideal reference samples were not available during our study, namely photonic crystals with a smaller lattice parameter such that emission is in the low-frequency limit, as discussed in Ref.[83] and shown in Figure 2.

In Figure 9(a) we see that the relative intensities for two different crystals with pore radii $R = 129$ nm reveal a strong inhibition between about 8000 and 10200 cm^{-1}, in very good mutual agreement. The very good reproducibility confirms that both the photonic crystal fabrication and the quantum dot infiltration method are also well reproduced. The minimum relative emission near 8800 cm^{-1} is about 0.2 to 0.25, corresponding to maximum inhibitions in the photonic band gap of 4 to 5-fold, relative to the reference situation described above. The theoretical DOS has a gap between 8000 and 10200 cm^{-1}, in very good agreement with the observations. Indeed, the (relative) pore radii pertaining to the calculations $R/a = 0.19$ agree well with pore radii derived from the SEM images and the radii used in the sample design.

Figure 9(b) shows the relative intensities for three other crystals that all have larger pore radii $R = 320$ nm than the crystals in panel (a). All three crystals reveal a strong inhibition between about 8000 and 10400 cm^{-1}, in very good mutual agreement. The inhibition of one crystal (green) amounts to about 10-fold, whereas the other two reveal a striking inhibition as large as 30-fold.

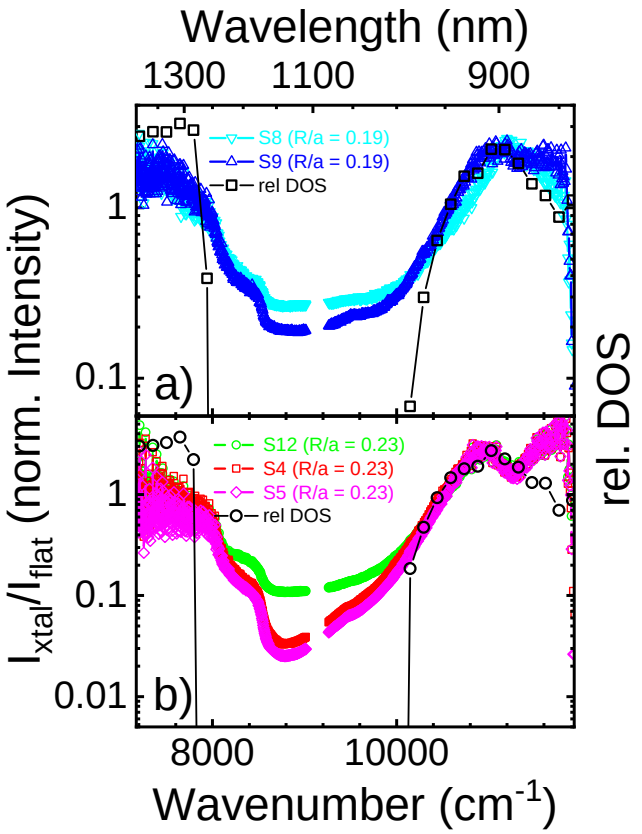

Figure 9: Normalized emission spectra of 3D photonic crystals on bar 3DPC1: (a) S9 (blue upward triangles), S8 (teal downward triangles), (b) S4 (red squares), S12 (green circles), and S5 (magenta diamonds). The ratio of the spectra measured on the structures and the flat reference spectrum is plotted versus photon energy in wavenumbers, and wavelength (top abscissa). Connected black open symbols are the theoretically calculated relative DOS, for relative pore radii (a) $R/a = 0.19$ and (b) $R/a = 0.23$.

In view of possible systematic experimental errors (like alignment and such), we estimate the overall inhibition to be 20 ± 10-fold. The theoretical DOS has a gap between 7900 and 10200 cm^{-1}, again in very good agreement with the observations, where, the (relative) pore radii pertaining to the calculations are indeed larger, namely $R/a = 0.23$ as in the experiments. In addition, referring back to Fig-

ure 2(b), it is remarkable that also the shape of the measured relative emission spectrum matches well with the shape of the theoretically calculated DOS.

The greater inhibition observed for the second set of crystals (in panel (b)) compared to the first makes intuitive sense since the observed inhibition gap is wider. Moreover, the reduced pore radii of the second set of crystals is closer to the value $R/a = 0.245$ that is known to reveal the broadest 3D photonic band gaps in inverse woodpile photonic crystals made from silicon.[68,89]

Discussion and outlook

The inhibition in 3D inverse woodpile crystals was previously studied by Leistikow *et al.* in time-resolved studies on high-quantum efficiency quantum dots randomly infiltrated throughout the pores.[31] Leistikow *et al.* observed an inhibition of about 10-fold, which agrees remarkably well with our present results. We speculate that this agreement is coincidental, in view of several notable differences between both studies. Firstly, in the present study the quantum dots are positioned by the polymer brushes to a limited set of positions in the unit cell (near the axes of the pores, see Figure3(b)), whereas Leistikow *et al.* infiltrated the quantum dots as a suspension in the pores hence their quantum dots sample all spatial positions in the pores and thus many more positions in the unit cell, namely about 80% of the whole volume. From theory it is known that the local density of states (LDOS) at a single position varies much more strongly with frequency (thus yielding more inhibition) than when such the LDOS is averaged over many more positions inside a photonic crystal's unit cell, when in the extreme case of all positions the averaged LDOS becomes the DOS, which yields a smoother result, see Refs.[62,77] Secondly, here we study time-averaged emission of low-efficiency quantum dots whereas Leistikow *et al.* studied time-resolved emission of high-efficiency dots; the second technique allows to distinguish between different dynamics in a population of quantum emitters (see van Driel *et al.*[90]), whereas a time-average study reveals an average emission rate. Within a distribution of emission rates that is accessible by time-resolved studies, one may thus find more variable emission rates, whereas averaged rates are usually much smoother. A third notable difference is that Leistikow *et al.* kept their quantum dots in (toluene) suspension, as a result of which the refractive index ratio with the silicon backbone is less, hence the photonic band gap is narrower, and hence the inhibition is reduced. In the present study, the quantum dots are attached to the brush polymers inside the pores; it is speculated that the overall density of material inside the pores, see the schematic cross-section in Figure 3, also increases the dielectric function ϵ inside the pores. This hypothesis is inspired by the observation in our previous X-ray imaging study that tomography (by elastic scattered X-rays) was not feasible due to too little contrast in electron density between the silicon backbone and the filled pores.[66] In summary, compared to the work of Leistikow *et al.*, the reasons above could respectively result in increased, decreased, and similar decay rates, hence the similar observed inhibition seems coincidental to us.

The inhibition of quantum emitters was also studied on completely different 3D photonic crystals.[25,26,30,91] In TiO_2 inverse opal photonic crystals made by self-assembly,[92] Koenderink *et al.* observed a broadband angle-integrated inhibition in the emission spectra of laser dye by 5-fold.[25,83] The inhibition is likely less than observed here in view of the fact that TiO_2 photonic crystals have a lower refractive index contrast than our Si nanostructures, combined with the feature that these inverse opals do not possess a full 3D band gap, as opposed to our photonic crystals. In GaAs woodpile photonic crystals, Ogawa *et al.* reported an inhibition of 45-fold on embedded quantum wells.[26] While the index contrast of GaAs nanostructures is nearly the same as in our Si crystals, the inhibition is slightly larger than observed here, which we attribute to the

feature that their emitters are only located in the central layer of the woodpile structure and thus well-shielded, whereas in the present case the emitters are located over the whole length of the pores and thus also near the crystal surface where they are less shielded from the vacuum. Li *et al*. studied PbS quantum dots in polymer photonic crystals and reported an inhibition of 20%.[91] It is reasonable that this inhibition is less than observed here in view of the lower index contrast and concomitant absence of a full photonic band gap. Jorgensen *et al*. studied quantum dots in TiO_2 photonic crystals and observed inhibitions of about 4-fold,[30] which is also reasonably less than our observations in view of the lower index contrast and concomitant absence of a full photonic band gap. Taken together, all results confirm the long-standing expectation that substantial control of emission of embedded quantum emitters requires nanostructures with high-index semiconductors as backbone, in order to have sufficient refractive index contrast and preferably even a full 3D band gap.

As future extensions of our current study, it will firstly be relevant to calculate the LDOS for the positions where we detected the quantum dots to reside using X-ray imaging. Since it is therefore necessary to introduce X-ray imaging data into numerical *ab initio* computations of Maxwell's equations, it will be relevant to extend the recent method by Corbijn van Willenswaard *et al*. who describe a computational framework to introduce X-ray imaging data into computations.[93] Secondly, to allow for time-resolved studies with quantum dots positioned by brush polymers, it will be important to avoid the steps that induce quenching of the quantum efficiency of the dots. The most important step will be to avoid the copper catalysts, for instance, by invoking copper-free ATRP.[94] In addition, it will be relevant to design strategies to shield the quantum dots from oxygen and water, that are also well-known quenchers of highly efficient quantum dots, see *e.g.*, the experimental details in Refs.[27,95] Thirdly, the presence of brush polymers offers in future a very exciting prospect, namely to employ the length actuation of the brushes by physico-chemical means.[96–98] As a result, it may be feasible to tune or even switch the LDOS, the emission rate, and the inhibition by actuating the brushes. This in turn opens prospects to employing such actuated quantum emitters as sensitive position or pH-sensors or as novel platforms for tunable (photo)-chemistry.

Acknowledgments

We thank Cock Harteveld for technical support and sample fabrication, Christian Blum for helpful discussions, Ravitej Uppu and Matthijs Velsink for experimental help, Elahe Yeganegi for the cartoon in Figure 1, and Timon Vreman for help and comments and Melissa Goodwin for helpful comments. This work was supported by the project "Tunable light sources by positioning quantum dots in 3D photonic bandgap crystals with polymer brushes" (712.012.003) of the "Nederlandse Organisatie voor Wetenschappelijk Onderzoek" (NWO), and by NWO-TTW Perspectief program P15-36 "Free-form scattering optics" (FFSO) in collaboration with TUE and TUD and with industrial partners ASML, Demcon, Lumileds, Schott, Signify, and TNO.

References

(1) Bykov, V. P. Spontaneous Emission in a Periodic Structure. *Journal Theor. Exp. Physics* **1972**, *62*, 269.

(2) Yablonovitch, E. Inhibited Spontaneous Emission in Solid-State Physics and Electronics. *Phys. Rev. Lett.* **1987**, *58*, 2059–2062.

(3) Tandaechanurat, A.; Ishida, S.; Guimard, D.; Nomura, M.; Iwamoto, S.; Arakawa, Y. Lasing oscillation in a three-dimensional photonic crystal nanocavity with a complete bandgap. *Nature Photon.* **2011**, *5*, 91–94.

(4) Barnes, W. L.; Björk, G.; Gérard, J.-M.; Jonsson, P.; Wasey, J.; Worthing, P.; Zwiller, V. Solid-state single photon sources: light collection strategies. *Eur. Phys. J. D* **2000**, *18*, 197–210.

(5) Pelton, M.; Santori, C.; Vučković, J.; Zhang, B.; Solomon, G. S.; Plant, J.; Yamamoto, Y. Efficient Source of Single Photons: A Single Quantum Dot in a Micropost Microcavity. *Phys. Rev. Lett.* **2002**, *89*, 233602.

(6) Lodahl, P.; Mahmoodian, S.; Stobbe, S. Interfacing single photons and single quantum dots with photonic nanostructures. *Rev. Mod. Phys.* **2015**, *87*, 347–400.

(7) Fleming, J. G.; Lin, S. Y.; El-Kady, I.; Biswas, R.; Ho, K.-M. All-metallic three-dimensional photonic crystals with a large infrared bandgap. *Nature (London)* **2002**, *471*, 52–55.

(8) Sharma, D.; Hasan, S. B.; Saive, R.; van der Vegt, J. J. W.; Vos, W. L. Enhanced absorption in thin and ultrathin silicon films by 3D photonic band gap back reflectors. *Opt. Express* **2021**, *29*, 41023–41047.

(9) Nishimura, S.; Abrams, N.; Lewis, B. A.; Halaoui, L. I.; Mallouk, T. E.; Benkstein, K. D.; van de Lagemaat, J.; Frank, A. J. Standing Wave Enhancement of Red Absorbance and Photocurrent in Dye-Sensitized Titanium Dioxide Photoelectrodes Coupled to Photonic Crystals. *Journal of the American Chemical Society* **2003**, *125*, 6306–6310.

(10) Li, H.; Liu, R.; Lian, S.; Liu, Y.; Huang, H.; Kang, Z. Near-infrared light controlled photocatalytic activity of carbon quantum dots for highly selective oxidation reaction. *NANOSCALE* **2013**, *5*, 3289–3297.

(11) Li, R.; Zhang, Y.; Tu, W.; Dai, Z. Photoelectrochemical Bioanalysis Platform for Cells Monitoring Based on Dual Signal Amplification Using in Situ Generation of Electron Acceptor Coupled with Heterojunction. *ACS Applied Materials & Interfaces* **2017**, *9*, 22289–22297.

(12) Frasco, M. F.; Chaniotakis, N. Semiconductor Quantum Dots in Chemical Sensors and Biosensors. *Sensors* **2009**, *9*, 7266–7286.

(13) Li, M.; Chen, T.; Gooding, J. J.; Liu, J. Review of Carbon and Graphene Quantum Dots for Sensing. *ACS Sensors* **2019**, *4*, 1732–1748, PMID: 31267734.

(14) Haroche, S. In *Fundamental systems in quantum optics*; Dalibard, J., Raimond, J. M., Zinn-Justin, J., Eds.; North Holland, Amsterdam, 1992; pp 767–940.

(15) Milonni, P. W. *The Quantum Vacuum: an Introduction to Quantum Electrodynamics*; Academic Press, Boston, 1994.

(16) Purcell, E. M. Spontaneous emission probabilities at radio frequencies. *Phys. Rev.* **1946**, *69*, 681.

(17) Soukoulis, C. M., Ed. *Photonic Crystals and Light Localization in the 21st century*; Kluwer, Dordrecht, 2001.

(18) Novotny, L.; Hecht, B. *Principles of Nano-Optics*; Cambridge University Press: Cambridge, 2006.

(19) Lourtioz, J.-M.; Benisty, H.; Berger, V.; Gérard, J.-M.; Maystre, D.; Tchelnokov, A.; Pagnoux, D. *Photonic Crystals*; Springer Berlin Heidelberg: Berlin, Heidelberg, 2008.

(20) Ghulinyan, M., Pavesi, L., Eds. *Light Localisation and Lasing*; Cambridge University Press: Cambridge, 2015.

(21) Barnes, W. L.; Horsley, S. A. R.; Vos, W. L. Classical antennas, quantum emitters, and densities of optical states. *Journal of Optics* **2020**, *22*, 073501.

(22) Blanco, A.; López, C.; Mayoral, R.; Míguez, H.; Meseguer, F.; Mifsud, A.; Herrero, J. CdS photoluminescence inhibition by a photonic structure. *Appl. Phys. Lett.* **1998**, *73*, 1781–1783.

(23) Yamasaki, T.; Tsutsui, T. Spontaneous emission from fluorescent molecules embedded in photonic crystals consisting of polystyrene microspheres. *Appl. Phys. Lett.* **1998**, *72*, 1957–1959.

(24) Megens, M.; Wijnhoven, J. E. G. J.; Lagendijk, A.; Vos, W. L. Fluorescence lifetimes and linewidths of dye in photonic crystals. *Phys. Rev. A* **1999**, *59*, 4727–4731.

(25) Koenderink, A. F.; Bechger, L.; Schriemer, H.; Lagendijk, A.; Vos, W. L. Broadband fivefold reduction of vacuum fluctuations probed by dyes in photonic crystals. *Physical review letters* **2002**, *88*, 143903.

(26) Ogawa, S.; Imada, M.; Yoshimoto, S.; Okano, M.; Noda, S. Control of light emission by 3D photonic crystals. *Science* **2004**, *305*, 227–229.

(27) Lodahl, P.; van Driel, A. F.; Nikolaev, I. S.; Irman, A.; Overgaag, K.; Vanmaekelbergh, D.; Vos, W. L. Controlling the dynamics of spontaneous emission from quantum dots by photonic crystals. *Nature* **2004**, *430*, 654–657.

(28) Vallée, R. A. L.; Baert, K.; Kolaric, B.; Van der Auweraer, M.; Clays, K. Nonexponential decay of spontaneous emission from an ensemble of molecules in photonic crystals. *Phys. Rev. B* **2007**, *76*, 045113.

(29) Vion, C.; Barthou, C.; Bénalloul, P.; Schwob, C.; Coolen, L.; Gruzintev, A.; Emel'chenko, G.; Masalov, V.; Frigerio, J.-M.; Maître, A. Manipulating emission of CdTeSe nanocrystals embedded in three-dimensional photonic crystals. *J. Appl. Phys.* **2009**, *105*, 113120.

(30) Jorgensen, M. R.; Galusha, J. W.; Bartl, M. H. Strongly Modified Spontaneous Emission Rates in Diamond-Structured Photonic Crystals. *Phys. Rev. Lett.* **2011**, *107*, 143902.

(31) Leistikow, M. D.; Mosk, A. P.; Yeganegi, E.; Huisman, S. R.; Lagendijk, A.; Vos, W. L. Inhibited Spontaneous Emission of Quantum Dots Observed in a 3D Photonic Band Gap. *Phys. Rev. Lett.* **2011**, *107*, 193903: 1–5.

(32) Arcari, M.; Söllner, I.; Javadi, A.; Lindskov Hansen, S.; Mahmoodian, S.; Liu, J.; Thyrrestrup, H.; Lee, E. H.; Song, J. D.; Stobbe, S. et al. Near-Unity Coupling Efficiency of a Quantum Emitter to a Photonic Crystal Waveguide. *Phys. Rev. Lett.* **2014**, *113*, 093603.

(33) Tajiri, T.; Takahashi, S.; Ota, Y.; Watanabe, K.; Iwamoto, S.; Arakawa, Y. Three-dimensional photonic crystal simultaneously integrating a nanocavity laser and waveguides. *Optica* **2019**, *6*, 296–299.

(34) Takahashi, S.; Ota, Y.; Tajiri, T.; Tatebayashi, J.; Iwamoto, S.; Arakawa, Y. Circularly polarized vacuum field in three-dimensional chiral photonic crystals probed by quantum dot emission. *Phys. Rev. B* **2017**, *96*, 195404.

(35) Goy, P.; Raimond, J. M.; Gross, M.; Haroche, S. Observation of Cavity-Enhanced Single-Atom Spontaneous

Emission. *Phys. Rev. Lett.* **1983**, *50*, 1903–1906.

(36) Martini, F. D.; Innocenti, G.; Jacobovitz, G. R.; Mataloni, P. Anomalous Spontaneous Emission Time in a Microscopic Optical Cavity. *Phys. Rev. Lett.* **1987**, *59*, 2955–2958.

(37) Gérard, J.; Sermage, B.; Gayral, B.; Legrand, B.; Costard, E.; Thierry-Mieg, V. Enhanced Spontaneous Emission by Quantum Boxes in a Monolithic Optical Microcavity. *Phys. Rev. Lett.* **1998**, *81*, 1110–1113.

(38) Riboli, F.; Uccheddu, F.; Monaco, G.; Caselli, N.; Intonti, F.; Gurioli, M.; Skipetrov, S. E. Tailoring Correlations of the Local Density of States in Disordered Photonic Materials. *Phys. Rev. Lett.* **2017**, *119*, 043902.

(39) Treussart, F.; Hare, J.; Collot, L.; Lefèvre, V.; Weiss, D. S.; Sandoghdar, V.; Raimond, J. M.; Haroche, S. Quantized atom-field force at the surface of a microsphere. *Opt. Lett.* **1994**, *19*, 1651.

(40) Mabuchi, H.; Kimble, H. J. Atom galleries for whispering atoms: binding atoms in stable orbits around an optical resonator. *Opt. Lett.* **1994**, *19*, 749.

(41) Sandoghdar, V.; Treussart, F.; Hare, J.; Lefèvre-Seguin, V.; Raimond, J. M.; Haroche, S. Very low threshold whispering-gallery-mode microsphere laser. *Phys. Rev. A* **1996**, *54*, R1777–R1780.

(42) Anger, P.; Bharadwaj, P.; Novotny, L. Enhancement and Quenching of Single-Molecule Fluorescence. *Phys. Rev. Lett.* **2006**, *96*, 113002.

(43) Muskens, O. L.; Giannini, V.; Sánchez-Gil, J. A.; Gómez Rivas, J. Strong Enhancement of the Radiative Decay Rate of Emitters by Single Plasmonic Nanoantennas. *Nano Lett.* **2007**, *7*, 2871–2875.

(44) Rose, A.; Hoang, T. B.; McGuire, F.; Mock, J. J.; Ciracì, C.; Smith, D. R.; Mikkelsen, M. H. Control of Radiative Processes Using Tunable Plasmonic Nanopatch Antennas. *Nano Lett.* **2014**, *14*, 4797–4802.

(45) Hoang, T. B.; Akselrod, G. M.; Argyropoulos, C.; Huang, J.; Smith, D. R.; Mikkelsen, M. H. Ultrafast spontaneous emission source using plasmonic nanoantennas. *Nat. Commun.* **2015**, *6*, 7788.

(46) Chikkaraddy, R.; de Nijs, B.; Benz, F.; Barrow, S. J.; Scherman, O. A.; Rosta, E.; Demetriadou, A.; Fox, P.; Hess, O.; Baumberg, J. J. Single-molecule strong coupling at room temperature in plasmonic nanocavities. *Nature* **2016**, *535*, 127–130.

(47) Noginov, M. A.; Li, H.; Barnakov, Y. A.; Dryden, D.; Nataraj, G.; Zhu, G.; Bonner, C. E.; Mayy, M.; Jacob, Z.; Narimanov, E. E. Controlling spontaneous emission with metamaterials. *Opt. Lett.* **2010**, *35*, 1863.

(48) Lu, D.; Kan, J. J.; Fullerton, E. E.; Liu, Z. Enhancing spontaneous emission rates of molecules using nanopatterned multilayer hyperbolic metamaterials. *Nat. Nanotechnol.* **2014**, *9*, 48–53.

(49) Sharma, S.; Nair, R. V. Nanophotonic control of the color center emission from nanodiamonds. *Opt. Lett.* **2018**, *43*, 3989–3992.

(50) Yang, Z.; Pelton, M.; Bodnarchuk, M. I.; Kovalenko, M. V.; Waks, E. Spontaneous emission enhancement of colloidal perovskite nanocrystals by a photonic crystal cavity. *Applied Physics Letters* **2017**, *111*, 221104.

(51) Weisskopf, V.; Wigner, E. Berechnung der natürlichen Linienbreite auf Grund der Diracschen Lichttheorie. *Zeitschrift für Phys.* **1930**, *63*, 54–73.

(52) Fermi, E. Quantum Theory of Radiation. *Rev. Mod. Phys.* **1932**, *4*, 87–132.

(53) Clerk, A. A.; Devoret, M. H.; Girvin, S. M.; Marquardt, F.; Schoelkopf, R. J. Introduction to quantum noise, measurement, and amplification. *Rev. Mod. Phys.* **2010**, *82*, 1155–1208.

(54) Wubs, M.; Vos, W. L. Förster resonance energy transfer rate in any dielectric nanophotonic medium with weak dispersion. *New J. Phys.* **2016**, *18*, 053037.

(55) Snoeks, E.; Lagendijk, A.; Polman, A. Measuring and Modifying the Spontaneous Emission Rate of Erbium near an Interface. *Phys. Rev. Lett.* **1995**, *74*, 2459–2462.

(56) Sprik, R.; van Tiggelen, B. A.; Lagendijk, A. Optical emission in periodic dielectrics. *Europhys. Lett.* **1996**, *35*, 265.

(57) John, S.; Wang, J. Quantum electrodynamics near a photonic band gap: Photon bound states and dressed atoms. *Phys. Rev. Lett.* **1990**, *64*, 2418–2421.

(58) Busch, K.; John, S. Photonic band gap formation in certain self-organizing systems. *Phys. Rev. E* **1998**, *58*, 3896–3908.

(59) Li, Z.-Y.; Xia, Y. Full vectorial model for quantum optics in three-dimensional photonic crystals. *Phys. Rev. A* **2001**, *63*, 043817.

(60) Vats, N.; John, S.; Busch, K. Theory of fluorescence in photonic crystals. *Phys. Rev. A* **2002**, *65*, 043808.

(61) Wang, X.-H.; Gu, B.-Y.; Wang, R.; Xu, H.-Q. Decay Kinetic Properties of Atoms in Photonic Crystals with Absolute Gaps. *Phys. Rev. Lett.* **2003**, *91*, 113904.

(62) Nikolaev, I. S.; Vos, W. L.; Koenderink, A. F. Accurate calculation of the local density of optical states in inverse-opal photonic crystals. *J. Opt. Soc. Am. B* **2009**, *26*, 987–997.

(63) Economou, E. N. *The Physics of Solids*; Graduate Texts in Physics; Springer Berlin Heidelberg: Berlin, Heidelberg, 2010.

(64) Matyjaszewski, K.; Xia, J. Atom Transfer Radical Polymerization. *Chemical Reviews* **2001**, *101*, 2921–2990, PMID: 11749397.

(65) Lee, H.-i.; Pietrasik, J.; Sheiko, S. S.; Matyjaszewski, K. Stimuli-responsive molecular brushes. *Progress in Polymer Science* **2010**, *35*, 24–44.

(66) Schulz, A. S.; Harteveld, C. A. M.; Vancso, G. J.; Huskens, J.; Cloetens, P.; Vos, W. L. Targeted positioning of quantum dots inside 3D silicon photonic crystals revealed by synchrotron X-ray fluorescence tomography. *ACS Nano* **2022**, *16*, 3674–3683.

(67) Ho, K. M.; Chan, C. T.; Soukoulis, C. M.; Biswas, R.; Sigalas, M. Photonic Band Gaps in Three Dimensions: New Layer-By-Layer Periodic Structures. *Solid State Commun.* **1994**, *89*, 413–416.

(68) Woldering, L. A.; Mosk, A. P.; Tjerkstra, R. W.; Vos, W. L. The Influence of Fabrication Deviations on the Photonic Band Gap of Three-Dimensional Inverse Woodpile Nanostructures. *J. Appl. Phys.* **2009**, *105*, 093108.

(69) Huisman, S. R.; Nair, R. V.; Woldering, L. A.; Leistikow, M. D.; Mosk, A. P.; Vos, W. L. Signature of a three-dimensional photonic band gap observed on silicon inverse woodpile photonic crystals. *Phys. Rev. B* **2011**, *83*, 205313.

(70) Moreels, I.; Lambert, K.; Smeets, D.; De Muynck, D.; Nollet, T.; Martins, J. C.; Vanhaecke, F.; Vantomme, A.; Delerue, C.; Allan, G. et al. Size-Dependent Optical Properties of Colloidal PbS Quantum Dots. *ACS Nano* **2009**, *3*, 3023–3030, PMID: 19780530.

(71) Peng, X.; Wickham, J.; Alivisatos, A. Kinetics of II-VI and III-V colloidal semiconductor nanocrystal growth:'Focusing'of size distributions. *Journal of the American Chemical Society* **1998**, *120*.

(72) Bohren, C. F.; Huffman, D. R. *Absorption and Scattering of Light by Small Particles*; John Wiley & Sons, 1998.

(73) Lakowicz, J. R. *Principles of Fluorescence Spectroscopy, 3rd Edition*; Springer, Berlin, 2006.

(74) Fox, M. *Optical Properties of Solids, 2nd Ed.*; Oxford University Press, 2010.

(75) Förster, T. Zwischenmolekulare Energiewanderung und Fluoreszenz. *Ann. Phys.* **1948**, *437*, 55–75.

(76) Koenderink, A. F.; Lagendijk, A.; Vos, W. L. Optical extinction due to intrinsic structural variations of photonic crystals. *Physical Review B* **2005**, *72*, 153102.

(77) Mavidis, C. P.; Tasolamprou, A. C.; Hasan, S. B.; Koschny, T.; Economou, E. N.; Kafesaki, M.; Soukoulis, C. M.; Vos, W. L. Local density of optical states in the three-dimensional band gap of a finite photonic crystal. *Phys. Rev. B* **2020**, *101*, 235309.

(78) Franz, W. Einfluß eines elektrischen Feldes auf eine optische Absorptionskante. *Zeitschrift für Naturforschung A* **1958**, *13*, 484–489.

(79) Keldysh, L. V. Behavior of Non-metallic Crystals in Strong Electric Fields. *Soviet Journal of Experimental and Theoretical Physics* **1958**, *6*, 763.

(80) Tabernig, S. W.; Daiber, B.; Wang, T.; Ehrler, B. Enhancing silicon solar cells with singlet fission: the case for Förster resonant energy transfer using a quantum dot intermediate. *J. Photonics Energy* **2018**, *8*, 8 – 8 – 12.

(81) Tisdale, W. A.; Williams, K. J.; Timp, B. A.; Norris, D. J.; Aydil, E. S.; Zhu, X.-Y. Hot-Electron Transfer from Semiconductor Nanocrystals. *Science* **2010**, *328*, 1543–1547.

(82) Adhikary, M.; Uppu, R.; Harteveld, C. A. M.; Grishina, D. A.; Vos, W. L. Experimental probe of a complete 3D photonic band gap. *Opt. Express* **2020**, *28*, 2683–2698.

(83) Koenderink, A. F.; Bechger, L.; Lagendijk, A.; Vos, W. L. An experimental study of strongly modified emission in inverse opal photonic crystals. *physica status solidi (a)* **2003**, *197*, 648–661.

(84) El-Dardiry, R. G. S.; Faez, S.; Lagendijk, A. Classification of light sources and their interaction with active and passive environments. *Phys. Rev. A* **2011**, *83*, 031801.

(85) Nordin, M. N.; Li, J.; Clowes, S. K.; Curry, R. J. Temperature dependent optical properties of PbS nanocrystals. *Nanotechnology* **2012**, *23*, 275701.

(86) Justo, Y.; Geiregat, P.; van Hoecke, K.; Vanhaecke, F.; De Mello Donega, C.; Hens, Z. Optical Properties of PbS/CdS Core/Shell Quantum Dots. *The Journal of Physical Chemistry C* **2013**, *117*, 20171–20177.

(87) Chen, W.; Tu, X.; Guo, X. Fluorescent gold nanoparticles-based fluorescence sensor for Cu2+ ions. *Chem. Commun.* **2009**, 1736–1738.

(88) Sung, T.-W.; Lo, Y.-L. Highly sensitive and selective sensor based on silica-coated CdSe/ZnS nanoparticles for Cu2+ ion detection. *Sensors and Actuators B: Chemical* **2012**, *165*, 119–125.

(89) Hillebrand, R.; Senz, S.; Hergert, W.; Gösele, U. Macroporous-silicon-based three-dimensional photonic crystal with a large complete band gap. *Journal of Applied Physics* **2003**, *94*, 2758–2760.

(90) Van Driel, A. F.; Nikolaev, I. S.; Vergeer, P.; Lodahl, P.; Vanmaekelbergh, D.; Vos, W. L. Statistical analysis of time-resolved emission from ensembles of semiconductor quantum dots: Interpretation of exponential decay models. *Phys. Rev. B* **2007**, *75*, 035329.

(91) Li, J.; Jia, B.; Zhou, G.; Bullen, C.; Serbin, J.; Gu, M. Spectral Redistribution in Spontaneous Emission from Quantum-Dot-Infiltrated 3D Woodpile Photonic Crystals for Telecommunications. *Advanced Materials* **2007**, *19*, 3276–3280.

(92) Wijnhoven, J. E. G. J.; Vos, W. L. Preparation of Photonic Crystals Made of Air Spheres in Titania. *Science* **1998**, *281*, 802–804.

(93) Corbijn van Willenswaard, L.; Schlottbom, M.; van der Vegt, J. J. W.; Vos, W. L. Non-utopian optical properties computed of a tomographically reconstructed real photonic band gap crystal. *Preprint* **2023**,

(94) Treat, N. J.; Sprafke, H.; Kramer, J. W.; Clark, P. G.; Barton, B. E.; Read de Alaniz, J.; Fors, B. P.; Hawker, C. J. Metal-Free Atom Transfer Radical Polymerization. *Journal of the American Chemical Society* **2014**, *136*, 16096–16101, PMID: 25360628.

(95) Nikolaev, I. S.; Lodahl, P.; van Driel, A. F.; Koenderink, A. F.; Vos, W. L. Strongly nonexponential time-resolved fluorescence of quantum-dot ensembles in three-dimensional photonic crystals. *Phys. Rev. B* **2007**, *75*, 115302.

(96) Tagit, O.; Tomczak, N.; Benetti, E. M.; Cesa, Y.; Blum, C.; Subramaniam, V.; Herek, J. L.; Vancso, G. J. Temperature-modulated quenching of quantum dots covalently coupled to chain ends of poly(N-isopropyl acrylamide) brushes on gold. *Nanotechnology* **2009**, *20*, 185501.

(97) Roy, D.; Brooks, W. L. A.; Sumerlin, B. S. New directions in thermoresponsive polymers. *Chem. Soc. Rev.* **2013**, *42*, 7214–7243.

(98) Wei, M.; Gao, Y.; Li, X.; Serpe, M. J. Stimuli-responsive polymers and their applications. *Polym. Chem.* **2017**, *8*, 127–143.

Graphical TOC Entry